

Performance analysis of GaN based dual active bridge converter for electric vehicle charging application

Snehalika, Ranjeeta Patel, Chinmoy Kumar Panigrahi

School of Electrical Engineering, KIIT Deemed to be University, Bhubaneswar, India

Article Info

Article history:

Received Oct 18, 2023

Revised Nov 4, 2023

Accepted Nov 10, 2023

Keywords:

Dual active bridge

Electric vehicle

EV charging

Gallium Nitride

Silicon

ABSTRACT

The research work proposes a Gallium Nitride (GaN) based dual active bridge (DAB) converter for electric vehicle (EV) charging applications. The wide bandgap semiconductor device, GaN is implemented in the DAB topology of an Isolated Bidirectional DC-DC converter (IBDC). GaN-based DC-DC converters lead to higher efficiency, smaller size, faster charging, and reduced heat generation improving the overall performance of the EV charging system. The performance characteristics of GaN based DAB converter is analyzed both in simulation and hardware for EV charging application. The same analysis is extended to a Si based DAB converter and comparative results are presented. A 14.25 kW GaN based DAB and 10.5 kW Si based DAB is designed and evaluated using LTspice XVII software and a scaled-down prototype of 0.612 kW GaN based DAB and 0.25 kW Si based DAB is presented for experimental validation. Result analysis under similar operating conditions indicated an improvement of 36% more output power transfer on the GaN based DAB over the traditional Si based DAB. The developed prototype showcased improved levels of power, voltage, and current under same operating conditions. The power transmission in the developed DAB based IBDC topology is controlled using the Single-Phase-Shift (SPS) control strategy.

This is an open access article under the [CC BY-SA](https://creativecommons.org/licenses/by-sa/4.0/) license.



Corresponding Author:

Snehalika

School of Electrical Engineering, KIIT Deemed to be University

Bhubaneswar-751024, India

Email: snehalika.fel@kiit.ac.in

1. INTRODUCTION

Wide bandgap semiconductors, such as silicon carbide (SiC) and gallium nitride (GaN), have ushered in a transformative era in power electronics. These materials exhibit remarkable electrical properties that enable more efficient and high-performance electronic devices. In power electronics, SiC and GaN devices are replacing traditional silicon-based components due to their ability to handle higher voltages and temperatures while minimizing energy losses [1], [2]. This shift has revolutionized industries like electric vehicles, renewable energy, and data centers. With reduced size, weight, and heat generation, wide bandgap semiconductors not only increase energy efficiency but also enhance system reliability, ultimately paving the way for a greener and more electrified future [3]–[5]. In the electric vehicle industry, the preference for GaN devices over Si (silicon) is gaining momentum. GaN offers notable advantages, including higher power density, lower costs, and enhanced efficiency, making it a compelling choice for EV applications. This shift underscores GaN's pivotal role in advancing electric mobility [6].

The isolated bidirectional DC-DC converter (IBDC) stands as a widely adopted topology for EV charging applications [7]–[9] presented in Figure 1. Figures 1(a)–1(d) represent the various isolated bidirectional topologies of DC-DC converter for EV charging with different configurations of inductor (L)

and capacitor (C). Progress in semiconductor materials and high-frequency power conversion systems (HF PCSs) has enabled IBDCs to eliminate losses associated with traditional Si-based switches and the need for large, heavy LF transformers [10]–[12]. Among all the four topologies presented in Figure 1, the eight-switch dual active bridge (DAB) presented in Figure 1(b) is the most common IBDC topology for the EV charging system [13]–[17].

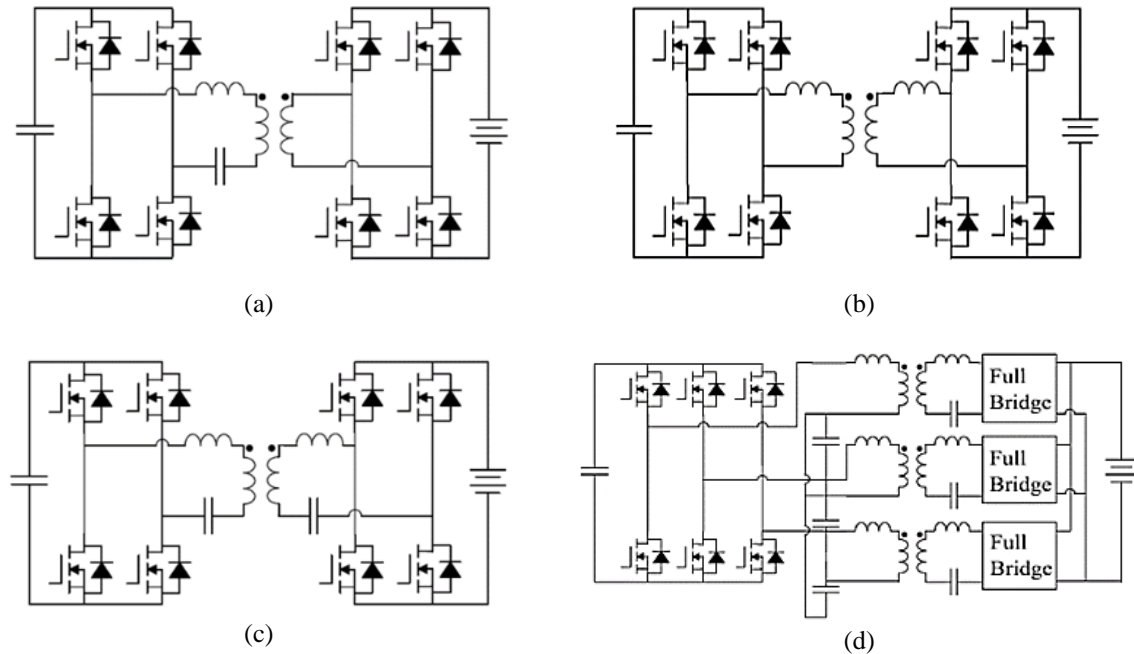


Figure 1. Isolated Bidirectional DC-DC (IBDC) topologies (a) Single-phase LLC, (b) Single-phase phase-shifted DAB, (c) Single-phase CLLC, and (d) Three-phase CLLC [17].

Si-based DAB converters have been widely adopted due to their mature technology, high voltage ratings, and well-established reliability. GaN-based DAB converters have gained significant attention in recent years due to their superior characteristics, including high switching speeds, low conduction losses, and high-power density [18]–[20]. This research paper aims to develop a GaN based DAB converter for EV charging applications. To confirm the functionality of the developed GaN based DAB converter, the simulation design is done using LTspice XVII software. Subsequently, a scaled-down prototype of 0.612 kW GaN based DAB is presented for an EV charging application to validate the proposed simulation model. The same analysis is extended to 0.25 kW prototype of Si based DAB for comparative analysis. The single-phase-shift control strategy is deployed for controlling power transmission in both converters. The research work in detail is arranged as follows. Section 2 proposes the developed DAB converters. Section 3 presents the results of simulation and experimental analysis. Section 4 concludes the paper.

2. PROPOSED GaN BASED DAB CONVERTER

This section presents the developed DAB converters with both GaN and Silicon semiconductor devices. The working principle of IBDC based DAB topology is also discussed in this section. The developed DAB converters are shown in Figures 2 and 3 by utilizing GaN and Silicon devices respectively. The primal contributions of the developed GaN based DAB are (i) high power operation, (ii) high efficiency as compared to conventional Si based DAB, and (iii) lower switching losses.

The input port is supplied via a DC-link voltage up to 600 V and the output port is designated to provide EV charging. Both the ports are coupled by a two-winding high frequency transformer (HFT). Each switch, S1-S8 has anti parallel diode, D1-D8 along with snubber capacitor, C1-C8 as shown in Figures 2 and 3 to aid in achieving zero voltage switching of the device [13], [21], [22]. The output port has a series inductor L_s . The primary winding turn is considered as unity, and the secondary is considered as N for the 2-winding HFT. The voltage at the primary of HFT is V_{py} and the secondary of HFT is V_{sy} with i_{L_s} as the inductor

current flowing in inductor, L_s . The DC-link voltage and input side current are V_{in} and I_{in} respectively. The parameters of the output port are output voltage and output current represented as V_o , and I_o respectively.

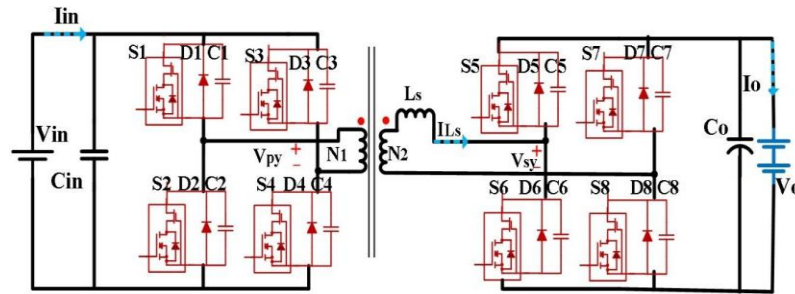


Figure 2. Circuit diagram of GaN-based DAB

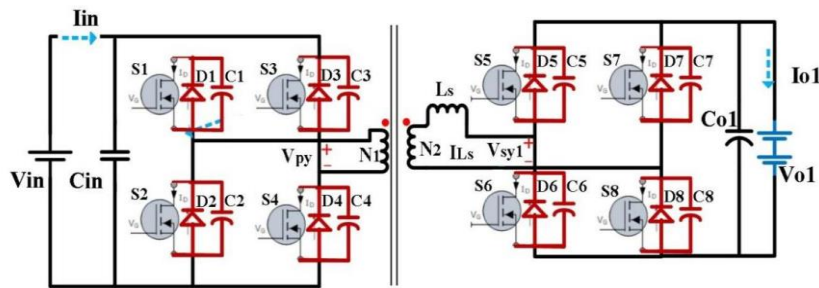


Figure 3. Circuit diagram of Si-based DAB

2.1. Working principle of DAB

The four modes of operation of the DAB converter indicating conducting switches are presented in Figure 4 as Mode I in Figure 4(a), Mode II in Figure 4(b), Mode III in Figure 4(c), and Mode IV in Figure 4(d). The theoretical waveform, V_{py} , V_{sy} and i_{Ls} of the DAB operating in Buck mode is presented in Figure 5.

Using (1), the voltage across the series inductor is given by the following expression [14].

$$v_{Ls} = L_s \cdot d \cdot \frac{i_{Ls}}{dt} \tag{1}$$

Where v_{Ls} and i_{Ls} represent voltages and currents across the series inductor L_s . The current flowing in the inductor at time intervals t_1 and t_2 can be given by $I_{(0)}$ and $I_{(d)}$ respectively where d is the phase-shift value. Both the current expression for $I_{(0)}$ and $I_{(d)}$ is provided in (2) and (3) respectively [14]. Mode I indicated in Figure 4(a) starts from t_1 as i_{Ls} increase from $I_{(0)}$.

$$I_{(0)} = T_s \cdot \frac{[N \cdot V_{in} + (2d-1)V_o]}{4L_s} \tag{2}$$

$$I_{(d)} = T_s \cdot \frac{[N \cdot V_{in} \cdot (2d-1) + V_o]}{4L_s} \tag{3}$$

Where T_s defines one time period. The different voltage levels obtained at primary and secondary of HFT and the status of conducting switches for all modes presented in Figure 4 are tabulated in Table 1. In solving (2) and (3), the output current for the output port is computed as (4).

$$I_o = \frac{N \cdot V_{in} \cdot (d-d^2)}{2L_s \cdot f} \tag{4}$$

The output current I_o directly depends on the value of phase-shift, turns-ratio, and input DC-link voltage and inversely varies with series inductance value and switching frequency. The voltage gain, g of the developed

DAB converter is designed to be unity using (5). The unity gain aids in achieving a full range of zero voltage switching (ZVS) operations [21], [22]. The DAB based IBDC topology has an inherent soft-switching capability. The series inductor values for the DAB converters can be computed considering (6) and is presented below [10].

$$g = \frac{V_o}{N \cdot V_{in}} \quad (5)$$

$$L_s \geq \frac{N \cdot V_{in} \cdot T_s}{2 \cdot I_o} (d - d^2) \quad (6)$$

The values of L_s considering the maximum value of d as 0.5 are computed to be 17.38 μH for GaN based DAB and 9 μH for the Si based DAB respectively.

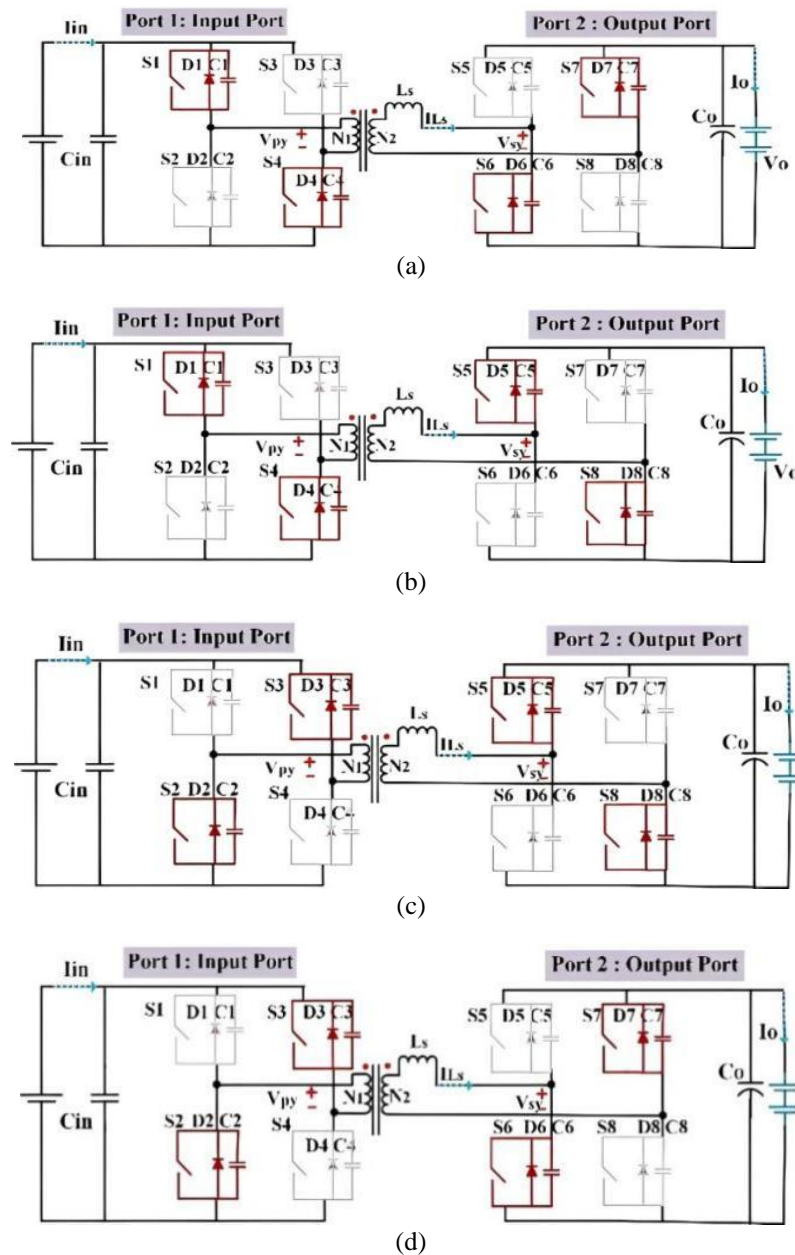


Figure 4. Four modes of operation of the DAB converter: (a) Mode I, (b) Mode II, (c) Mode III, and (d) Mode IV

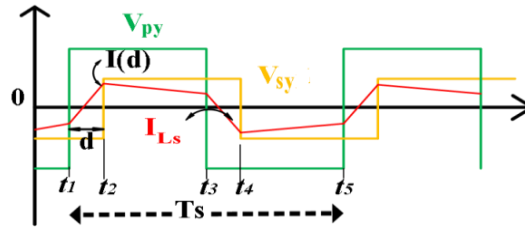


Figure 5. Operating waveform of DAB converter in Buck mode [13]

Table 1. Conduction status of switches S1-S8 in different modes

Ports/voltage level	Mode			
	I	II	III	IV
Input port	S1, S4	S1, S4	S2, S3	S2, S3
Output port	S6, S7	S5, S8	S5, S8	S6, S7
V_{py}	$+V_{in}$	$+V_{in}$	$-V_{in}$	$-V_{in}$
V_{sy}	$-V_o$	$+V_o$	$+V_o$	$-V_o$

2.2. Switching control strategy

The control strategy utilized for power transfer and control in the developed converter is the single-phase-shift (SPS) [23]. The SPS control method, which is depicted in Figure 5, is the most used control strategy for IBDC based DAB topology [24]–[26]. For the switches S1-S8 shown in Figures 2 and 3, PWM switching pulses are generated with a 50% duty ratio and at a constant operating frequency. The phase-shift value, d is varied to control the direction and magnitude of power flow between the input and output ports. The popularity of SPS control has been enhanced due to its simplicity in implementing the soft-switching control.

3. RESULTS AND DISCUSSION

3.1. Simulation results

The LTspice XVII simulation tool is used for validation of the designed GaN based DAB and Si based DAB converters. The converters are operated with a fixed duty ratio of 0.5 and different phase-shift values of 0.1, 0.167, 0.25, 0.33, and 0.4 for detailed analysis of output load parameters. This analysis is also extended over the Si based DAB for comparative analysis. The designed DAB converter parameters for a phase-shift value of 0.4 are listed in Table 2.

Figure 6 and Figure 7 present the simulation results at a phase-shift value of 0.4 for the GaN based DAB and Si based DAB converter respectively. The voltage at primary, V_{py} , and secondary, V_{sy} of the HFT, along with current, i_{Ls} through the series inductor presented in Figure 6(a) for the GaN based DAB. The output voltage, V_o and output current I_o , for the GaN based DAB converter is showcased in Figure 6(b) and Figure 6(c) indicating constant values of 475 V and 30 A respectively.

Table 2. Circuit Parameters for DAB converters

Parameters	Symbol	Value	
		GaN based	Si based
DC-link voltage (V)	V_{in}	600	600
Input current (A) (rms)	I_{in}	14.011	15.021
Load (Ω)	R_1	16.6	16.6
Average Output voltage (V)	V_o	475	420
Average Output current (A)	I_o	30	25
Output voltage ripple (V)	ΔV_o	0.91	0.7
Inductor current ripple (A)	ΔI_{Lout}	0.025	0.04
Output power (W)	P_o	14,250	10,500
Frequency (kHz)	f_s	50	50
Series inductor (μH)	L_s	17.38	9
Filter capacitor (μF)	C_1	470	470

The primary winding voltage V_{py} , and secondary winding voltage, V_{sy} of the HFT, along with current, i_{Ls} through the series inductor presented in Figure 7(a) for the Si based DAB. The output voltage, V_o and output current I_o , for the Si based DAB converter is showcased in Figure 7(b) and Figure 7(c) indicating

values of 420 V and 25 A respectively. The input current, I_{in} of the DAB converters is also presented in Figure 6(c) and Figure 7(c). Under the same operating conditions, the GaN based DAB converter was able to generate a power output of 14.25 kW compared to 10.25 kW by the Si based DAB converter which indicates an improvement of 36% more power transfer by the GaN based DAB.

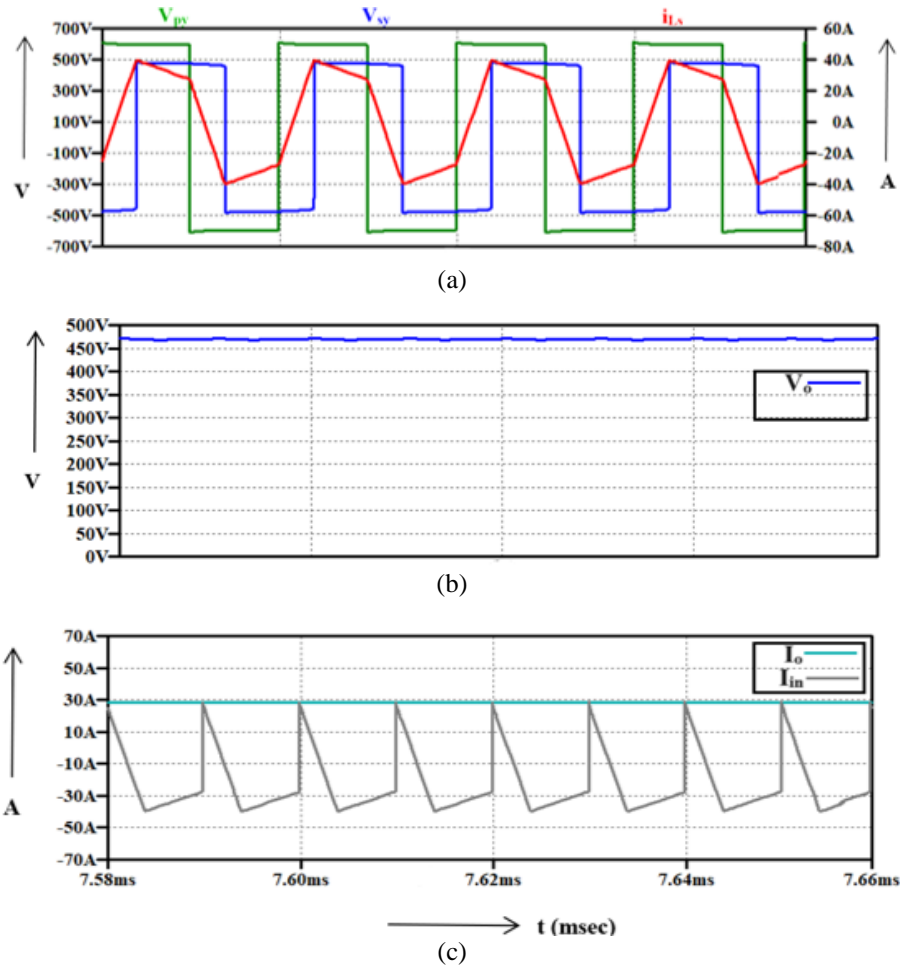


Figure 7. Simulation results for Si-based DAB: (a) voltages at the primary, V_{py} and secondary, V_{sy} winding of HFT and current, i_{Ls} , (b) average output voltage, V_o , and (c) average output current, I_o and input current, I_{in} .

3.2. Experimental results

Using the developed simulation model, a prototype of a 0.612 kW GaN based DAB and 0.25 kW Si based DAB converter has been developed and built as shown in Figure 8 and Figure 9 respectively. The GaN and Silicon MOSFET switching devices are taken from the manufacturers, Nexperia [27] and International Rectifier [26] respectively for carrying out the experimental analysis. The converter parameters are calculated utilizing the steady-state model stated in (1) to (6) in Section 2.1. Table 3 presents the parameters of the built prototype.

Table 3. Parameters for DAB prototype

Parameters	Symbol	Value	
		GaN	Si-MOSFET
Input DC-link voltage (V)	V_{in}	230	230
Average output voltage (V)	V_o	70	50
Average output current (A)	I_o	8.75	5
Output power (W)	P_o	612	250
Series inductor (μ H)	L_s	60	45
Turns-ratio	1/N	1:0.3	1:0.3

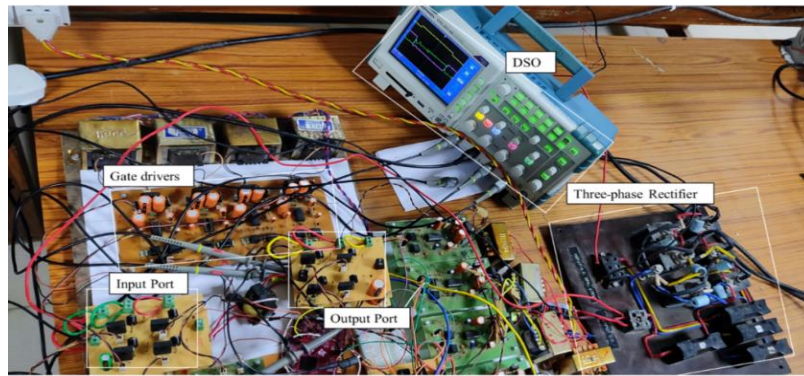


Figure 8. Prototype of 0.612 kW GaN based DAB converter

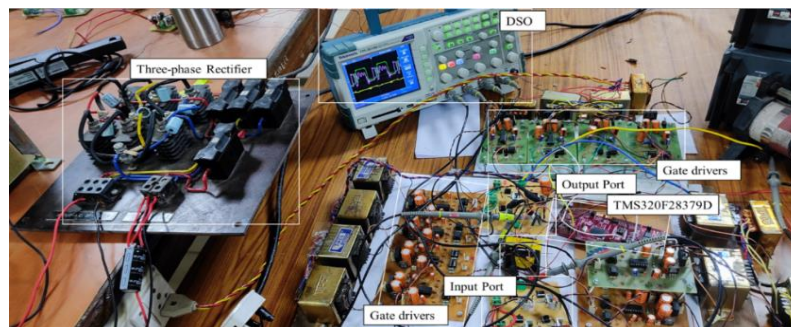


Figure 9. Prototype of 0.25 kW Si based DAB converter

The prototype model is supplied from a 3-phase rectifier operating with a maximum input voltage of 230 V to produce an output voltage and currents of 70 V, 8.75 A, and 50 V, 5 A at the output ports of the GaN based DAB and Si based DAB converter respectively. Figure 10 showcases the designed prototype of HFT. The HFT turn ratio, 1: N is designed for a maximum input voltage of 230 V, as 1:0.3.

The PWM pulses for switches S1-S8 are generated from a TMS320F28379D DSP processor. The recorded 50 kHz PWM pulses for switches S1-S4 of the primary bridge of DAB are presented in Figure 11. Figure 12 represents the phase-shifted 50 kHz PWM pulses with phase-shift introduced between switches of primary and secondary bridge of HFT. A same phase-shift value of 0.4 is introduced between switches S1 and S5 and S2 and S6 as shown in Figure 12. The experimental results for the developed GaN based DAB and Si based DAB are presented in Figure 13 and Figure 14 respectively. Figure 13 depicts the primary and secondary HFT voltage, V_{py} and, V_{sy} , load voltage, V_o of 70 V, and load current, I_o of 8.75A at the GaN based DAB converter in respect to the simulation results presented in Figure 6. Figure 14 depicts the primary and secondary HFT voltage, V_{py} and, V_{sy} , load voltage, V_o of 50 V and load current, and load current, I_o of 5A at the Si based DAB converter in respect to the simulation results presented in Figure 7.



Figure 10. Designed prototype of high frequency transformer (HFT)

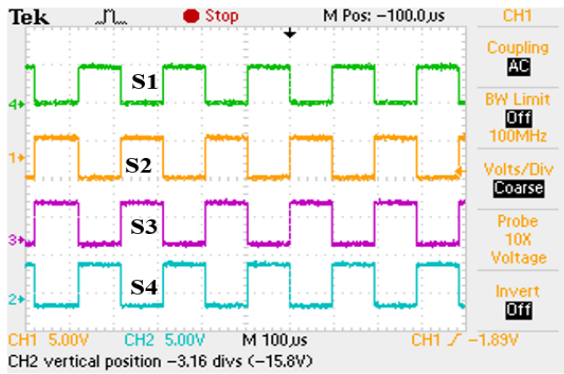


Figure 11. Switching pulses to switches, S1, S2, S3, and S4 of primary bridge

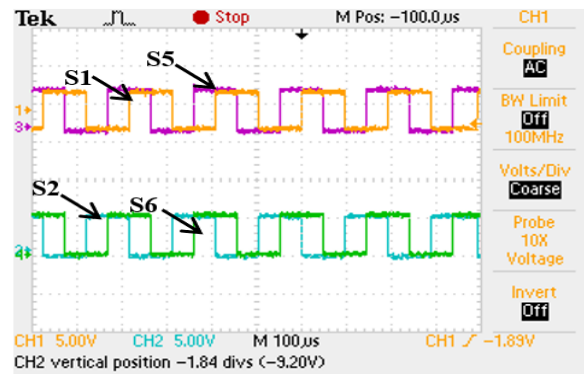


Figure 12. phase-shift value of 0.4 provided between switches S1, S5 and switches S2, S6

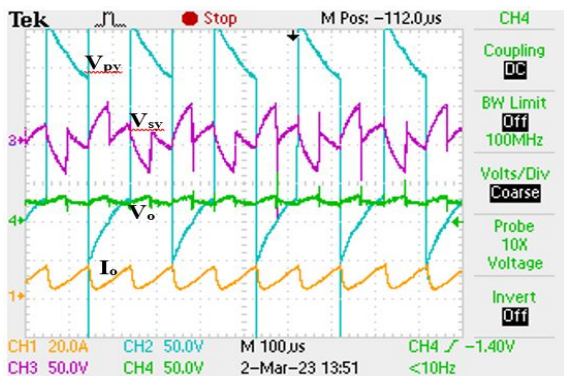


Figure 13. GaN based DAB: V_{py} , primary bridge and V_{sy} , secondary bridge voltage, load voltage, V_o of 70 V and load current, I_o of 8.75A

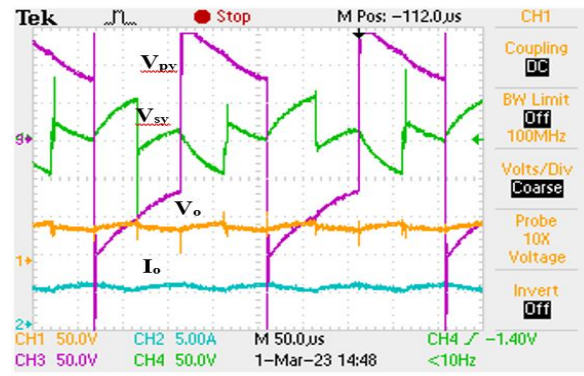


Figure 14. Si based DAB: V_{py} , primary bridge and V_{sy} , secondary bridge voltage, load voltage, V_o of 80 V and load current, I_o of 5 A

4. CONCLUSION




The performance characteristics of Gallium Nitride (GaN) based DAB and Si based DAB are examined on parameters of power transfer, voltage and current ratings. Simulation analysis with a DC-link voltage of 600 V is performed using LTspice XVII software for the GaN based DAB and Si based DAB converters with similar device rating of 650 V. The simulation analysis focused on evaluating the performance of both converters at a switching frequency of 50 kHz under the same operating conditions. The obtained results indicated an improvement of 36% more output power transfer on the GaN based DAB over the traditional Si based DAB. The obtained voltage levels at a phase-shift value of 0.4 were 475 V, and 420 V and the obtained current levels were 30 A, and 25 A respectively at the GaN based DAB and Si based DAB respectively. The total power output obtained is 14.25 kW and 10.5 kW on the GaN based and Si based DAB converters respectively. The experimental validation is carried out with a scaled-down prototype of 0.612 kW GaN based DAB and 0.25 kW Si based DAB converter. The prototype model of GaN based DAB achieved output voltage and current levels of 70 V, 8.75 A generating a total power of 0.612 kW. The prototype model of Si based DAB achieved output voltage, and current levels of 50 V, 5 A generating power of 0.250 kW. It is observed that the GaN based DAB outperforms the Si based DAB in terms of power transfer, output voltage, and current levels indicating GaN based devices are a better choice for EV applications. The SPS control strategy is utilized for controlling the power of developed converters.

REFERENCES




- [1] J. Millan, P. Godignon, X. Perpina, A. Perez-Tomas, and J. Rebollo, "A survey of wide bandgap power semiconductor devices," *IEEE Transactions on Power Electronics*, vol. 29, no. 5, pp. 2155–2163, 2014, doi: 10.1109/TPEL.2013.2268900.
- [2] U. K. Mishra, L. Shen, T. E. Kazior, and Y. F. Wu, "GaN-based RF power devices and amplifiers," *Proceedings of the IEEE*, vol. 96, no. 2, pp. 287–305, Feb. 2008, doi: 10.1109/JPROC.2007.911060.

- [3] E. A. Jones, F. F. Wang, and D. Costinett, "Review of commercial GaN power devices and GaN-based converter design challenges," *IEEE Journal of Emerging and Selected Topics in Power Electronics*, vol. 4, no. 3, pp. 707–719, Sep. 2016, doi: 10.1109/JESTPE.2016.2582685.
- [4] P. G. Neudeck, R. S. Okojie, and L.-Y. Chen, "High-temperature electronics - a role for wide bandgap semiconductors?," *Proceedings of the IEEE*, vol. 90, no. 6, pp. 1065–1076, Jun. 2002, doi: 10.1109/JPROC.2002.1021571.
- [5] R. S. Pengelly, S. M. Wood, J. W. Milligan, S. T. Sheppard, and W. L. Pribble, "A review of GaN on SiC high electron-mobility power transistors and MMICs," *IEEE Transactions on Microwave Theory and Techniques*, vol. 60, no. 6 PART 2, pp. 1764–1783, 2012, doi: 10.1109/TMTT.2012.2187535.
- [6] J. Lu *et al.*, "A modular-designed three-phase high-efficiency high-power-density EV battery charger using dual/triple-phase-shift control," *IEEE Transactions on Power Electronics*, vol. 33, no. 9, pp. 8091–8100, Sep. 2018, doi: 10.1109/TPEL.2017.2769661.
- [7] V. T. Tran, D. Sutanto, and K. M. Muttaqi, "The state of the art of battery charging infrastructure for electrical vehicles: Topologies, power control strategies, and future trend," in *2017 Australasian Universities Power Engineering Conference (AUPEC)*, IEEE, Nov. 2017, pp. 1–6. doi: 10.1109/AUPEC.2017.8282421.
- [8] S. Arulmozhi and K. R. Santha, "Review of multiport isolated bidirectional converter interfacing renewable and energy storage systems," *International Journal of Power Electronics and Drive Systems (IJPEDS)*, vol. 11, no. 1, pp. 466–476, 2020, doi: 10.11591/ijpeds.v11.i1.pp466-467.
- [9] M. Yilmaz and P. T. Krein, "Review of battery charger topologies, charging power levels, and infrastructure for plug-in electric and hybrid vehicles," *IEEE Transactions on Power Electronics*, vol. 28, no. 5, pp. 2151–2169, May 2013, doi: 10.1109/TPEL.2012.2212917.
- [10] S. Inoue and H. Akagi, "A bidirectional DC-DC converter for an energy storage system with galvanic isolation," *IEEE Transactions on Power Electronics*, vol. 22, no. 6, pp. 2299–2306, 2007, doi: 10.1109/TPEL.2007.909248.
- [11] B. Zhao, Q. Song, and W. Liu, "Power characterization of isolated bidirectional dual-active-bridge DC-DC converter with dual-phase-shift control," *IEEE Transactions on Power Electronics*, vol. 27, no. 9, pp. 4172–4176, Sep. 2012, doi: 10.1109/TPEL.2012.2189586.
- [12] S. S. Muthuraj, V. K. Kanakesh, P. Das, and S. K. Panda, "Triple phase shift control of an LLL tank based bidirectional dual active bridge converter," *IEEE Transactions on Power Electronics*, vol. 32, no. 10, pp. 8035–8053, Oct. 2017, doi: 10.1109/TPEL.2016.2637506.
- [13] M. N. Kheraluwala, R. W. Gascoigne, D. M. Divan, and E. D. Baumann, "Performance characterization of a high-power dual active bridge DC-to-DC converter," *IEEE Transactions on Industry Applications*, vol. 28, no. 6, pp. 1294–1301, 1992, doi: 10.1109/28.175280.
- [14] N. D. Dao, D.-C. Lee, and Q. D. Phan, "High-efficiency SiC-based isolated three-port DC/DC converters for hybrid charging stations," *IEEE Transactions on Power Electronics*, vol. 35, no. 10, pp. 10455–10465, Oct. 2020, doi: 10.1109/TPEL.2020.2975124.
- [15] T. Hirose, M. Takasaki, and Y. Ishizuka, "A power efficiency improvement technique for a bidirectional dual active bridge DC-DC converter at light load," *IEEE Transactions on Industry Applications*, vol. 50, no. 6, pp. 4047–4055, Nov. 2014, doi: 10.1109/TIA.2014.2327147.
- [16] S. Shao *et al.*, "Modeling and advanced control of dual-active-bridge DC-DC converters: a review index terms-DC-DC, dual active bridge (DAB), reduced-order model, generalized average model, discrete-time model, feedback control, feedforward control, model predictive control," *IEEE Transactions on Power Electronics*, vol. 37, no. 2, 2022, doi: 10.1109/TPEL.2021.
- [17] J. Yuan, L. Dorn-Gomba, A. D. Callegaro, J. Reimers, and A. Emadi, "A review of bidirectional on-board chargers for electric vehicles," *IEEE Access*, vol. 9, pp. 51501–51518, 2021, doi: 10.1109/ACCESS.2021.3069448.
- [18] R. Mitova, R. Ghosh, U. Mhaskar, D. Klikic, M.-X. Wang, and A. Dentella, "Investigations of 600-V GaN HEMT and GaN Diode for Power Converter Applications," *IEEE Transactions on Power Electronics*, vol. 29, no. 5, pp. 2441–2452, May 2014, doi: 10.1109/TPEL.2013.2286639.
- [19] Snehalika, R. Patel, C. K. Panigrahi, and A. K. Rathore, "High-power isolated bidirectional three-port DC-DC converter for level-1 and level-2 charging," in *2022 IEEE 2nd International Conference on Sustainable Energy and Future Electric Transportation (SeFeT)*, IEEE, Aug. 2022, pp. 1–6. doi: 10.1109/SeFeT55524.2022.9908861.
- [20] Snehalika, S. Das, R. Patel, and C. K. Panigrahi, "GaN-based isolated bi-directional DC-DC converter for high load current application," in *2022 IEEE Delhi Section Conference (DELCON)*, IEEE, Feb. 2022, pp. 1–7. doi: 10.1109/DELCON54057.2022.9753566.
- [21] L. Jin, B. Liu, and S. Duan, "ZVS soft switching operation range analysis of three-level dual-active bridge DC-DC converter under phase shift control strategy," *IEEE Transactions on Industry Applications*, vol. 55, no. 2, pp. 1963–1972, Mar. 2019, doi: 10.1109/TIA.2018.2872121.
- [22] K. S. Reddy and S. B. Veeranna, "Modified full bridge dual inductive coupling resonant converter for electric vehicle battery charging applications," *International Journal of Power Electronics and Drive Systems (IJPEDS)*, vol. 13, no. 2, p. 773, Jun. 2022, doi: 10.11591/ijpeds.v13.i2.pp773-782.
- [23] S. A. Gorji, H. G. Sahebi, M. Ektesabi, and A. B. Rad, "Topologies and Control Schemes of Bidirectional DC-DC Power Converters: An Overview," *IEEE Access*, vol. 7, pp. 117997–118019, 2019, doi: 10.1109/ACCESS.2019.2937239.
- [24] H. Bai, Z. Nie, and C. C. Mi, "Experimental comparison of Traditional phase-shift, dual-phase-shift, and model-based control of isolated bidirectional DC-DC converters," *IEEE Transactions on Power Electronics*, vol. 25, no. 6, pp. 1444–1449, Jun. 2010, doi: 10.1109/TPEL.2009.2039648.
- [25] M. A. Omar and M. M. Mahmoud, "Control of power converter used for electric vehicle DC charging station with the capability of balancing distribution currents and reactive power compensation," *International Journal of Power Electronics and Drive Systems (IJPEDS)*, vol. 12, no. 2, pp. 924–931, Jun. 2021, doi: 10.11591/ijpeds.v12.i2.pp924-931.
- [26] International Rectifier, "IRF640." pp. 2–9. Accessed: Jun. 18, 2021. [Online]. Available: <https://www.irf.com/product-info/datasheets/data/irf640.pdf>
- [27] Nexperia B.V., "650 V, 35 mΩ Gallium Nitride (GaN) FET in a TO-247 package. GAN041-650WSB datasheet." Accessed: Apr. 03, 2022. [Online]. Available: <https://assets.nexperia.com/documents/data-sheet/GAN041-650WSB.pdf>.




BIOGRAPHIES OF AUTHORS

Prof. Snehalika    is Assistant Professor at School of Electrical Engineering, Kalinga Institute of Industrial Technology Deemed to be University, Bhubaneswar, India. She is currently pursuing her Ph.D. degree in Electrical Engineering with specialization in Power electronics. She qualified GATE and received the M.Tech degree from NIT Warangal with specialization in Power Electronics and Drives. She received the B.Tech degree with specialization in Electronics and Electrical Engineering from KIIT, Deemed to be University. Her research areas are power electronics, DC-DC converters and Electric Vehicle charging. She has seven years of teaching experience in education and nine years teaching experience as a GATE trainer. She can be contacted at email: snehalika.fel@kiit.ac.in.



Dr. Ranjeeta Patel    is currently an Associate Professor with the School of Electrical Engineering, Kalinga Institute of Industrial Technology Deemed to be University, Bhubaneswar, India. She received the Ph.D. degree in electrical engineering from the National Institute of Technology Rourkela, India, in 2017. She has more than 10 years of teaching experience. Her research interests include applications of power electronics in power quality enhancement, active power filters, grid integration and renewable energy, fuzzy controller application, and electric vehicles. She can be contacted at email: ranjeeta.patelfel@kiit.ac.in.



Dr. Chinmoy Kumar Panigrahi    is currently Professor and Director, School of Electrical Engineering, KIIT DU. Prof. Panigrahi's research expertise lies in the field of Soft Computing Techniques, Power Systems, Renewable Energy, Battery Management System, Deregulation and Smart Grid. He has supervised 29 Ph.D. Scholars, 72 M.Tech. Scholars till date. He has published 182 research articles in referred Journals, presented 148 papers in reputed Conferences. He has won many accolades throughout his academic tenure of 32 years. He is also the Chair for IEEE Kolkata Section Industrial Electronics Society Chapter-Bhubaneswar and IEEE Kolkata Section Consumer Technology Society Chapter-Bhubaneswar as well. He is a senior member of the IEEE. He is a Fellow of Institution of Engineers (I), Life member for The Indian Society for Technical Education (ISTE); Fellow (Life) member for The Indian Society of Lighting Engineers (ISLE), Life Member of SESI, Member of IET and Member of Indian Science Congress (ISC). He can be contacted at email: chinmoy.panigrahifel@kiit.ac.in.